Journal of Innovative Optical Health Sciences
Vol. 3, No. 1 (2010) 45–51

World Scientific
www.worldscientific.com

LIMITATIONS OF CANCER MARGIN DELINEATION BY MEANS OF AUTOFLUORESCENCE IMAGING UNDER CONDITIONS OF LASER SURGERY

ALEXANDRE DOUPLIK*,§, AZHAR ZAM*, RALPH HOHENSTEIN†,
ANGELOS KALITZEOS*, EMEKA NKENKE‡ and FLORIAN STELZLE‡
*SAOT — Erlangen Graduate School in Advanced Optical Technologies
Friedrich-Alexander University Erlangen, Nuremberg, Germany
†Department of Photonic Technologies
Friedrich-Alexander University Erlangen, Nuremberg, Germany
‡Department of Oral and Maxillofacial Surgery
Friedrich-Alexander University Erlangen, Nuremberg, Germany
§alexandre.douplik@aot.uni-erlangen.de

Limitations of cancer margin delineation and surgical guidance by means of autofluorescence imaging under conditions of laser ablation were investigated and preliminary results are presented. PinPoint™ (Novadaq Technologies Inc., Canada) was used to capture digital images and Er:YAG laser (2.94 μm, Glissando, WaveLight™, Germany) was exploited to cause laser ablation on both normal and cancer sites of the specimen. It was shown that changes of the autofluorescence image after ablation extend beyond the actual sizes of the ablation loci. The tumor tissue after the laser ablation starts to emit fluorescent light within the green wavelength band (490–550 nm) similar to normal tissue stating that the current technology of in-process tissue classification fails. However, when the autofluorescence was collected in the red range (600–750 nm), then the abnormal/normal contrast was reduced, but still present even after the laser ablation. The present study highlights the importance of finding a proper technology for surgical navigation of cancer removal under conditions of high power effects in biological tissues.

Keywords: Cancer margin delineation; surgical guidance; surgical navigation; autofluorescence imaging; laser surgery; laser ablation.

1. Introduction

Remote laser surgery does not provide any haptic feedback during operation and surgical guidance is critically important at cancer resection. Image modalities such as spectral imaging, particularly fluorescence imaging,[1] narrow band imaging,[2] microendoscopy,[3] chromoendoscopy,[4] and chromomicroendoscopy,[5] infrared endoscopy[6] have been successfully applied in clinical practice for surgical navigation or guidance of cancer tumor resection in case when the malignancy cannot be delineated under white light observation. Autofluorescence imaging technique is an evolving adjunct to conventional white light examinations. The principle of autofluorescence endoscopy is to image the fluorescence of intrinsic fluorophores such as collagen, elastin, and NADH.[7,8] The difference in emitted fluorescence intensity and/or spectral composition between lesions and surrounding normal tissue provides the diagnostic contrast. The main concern of our preliminary study is an alteration of the contrast between cancerous and normal tissue

due to changes of optical tissue properties as a result of surgical interventions such as laser application. What is not clear is, how laser application affects the delineation contrast and what is more important, how eventually to provide better surgical navigation to control the cancer removal even under conditions of high power effects like coagulation and ablation. Laser surgery has a number of advantages including high precision, little trauma, and a high level of sterility. However, as any high power effect on the biological tissue such as ablation and hyperthermia, it changes its optical properties in terms of absorption,[9] scattering,[10,11] as well as both auto- and induced fluorescence.[12,13] The working hypothesis of the study was based on the notion that once the cancer tissue is removed then the tissue autofluorescence level will be recovered (Fig. 1). The first objective of this preliminary study was to assess the high power effects, such as laser ablation, and their influence on the cancer margin contrast in terms of autofluorescence imaging using a commercially available diagnostic system. The second objective was to explore, if the contrast of abnormal vs normal tissue can be maintained by processing the signals of the existing diagnostic system in an alternative way. And the third objective was to assess how the red fluorescence emission of abnormal tissue spots is altered by the ablation.

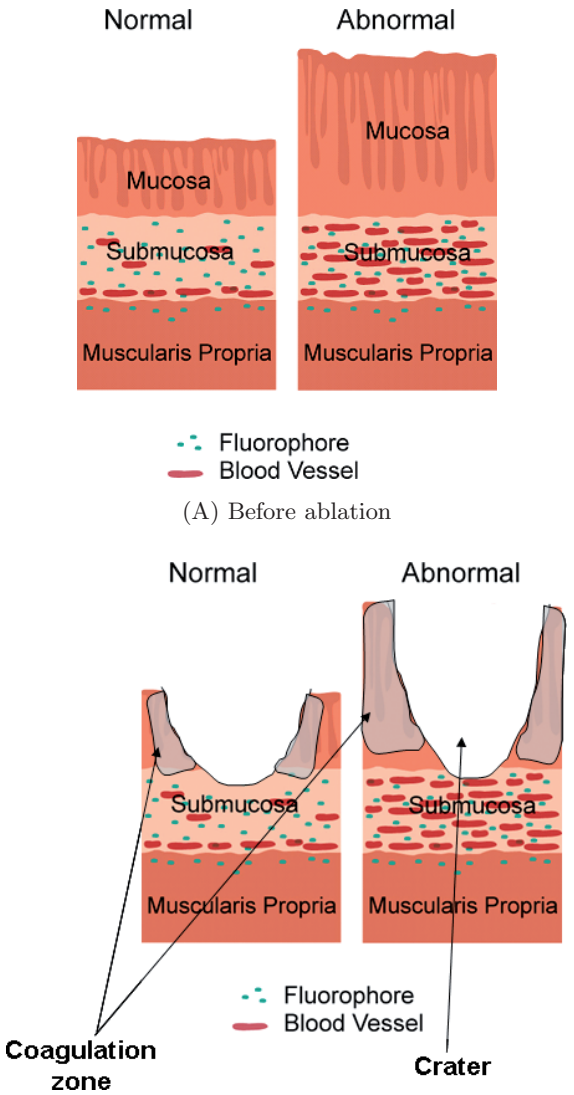

Fig. 1. Graphic representation of normal and cancerous tissues before (A) and after (B) ablation according to the recent notion of the surgical guidance via the fluorescence imaging. The ablation craters open up the tissue layers rich in fluorophores underneath the crater. The tissue autofluorescence increases and thus reduces the contrast between normal (bright) and abnormal (dull) areas.

2. Material and Methods

PinPoint^{TM} (Novadaq Technologies Inc., Canada) was used to capture digital images of human specimen of the lower jaw *ex vivo* where both normal and cancerous tissues were present (Fig. 2). PinPoint^{TM} is an endoscopic light source and video camera for use with conventional fiber endoscopes. Illumination for both WLE (white light endoscopy) and fluorescence endoscopy is provided by a super high-brightness mercury lamp (VIP R 150/P24, Osram, Germany). In fluorescence mode the green portion is suppressed by an optical filter, so that the output is a combination of the remaining blue and red light. The blue/red illuminating light is coupled into a fiberoptic endoscope, which projects it onto the tissue and collects the fluorescence (green) and diffuse reflectance (red) light. Optical filters block the reflected blue light and transmit the green and red images to the corresponding cameras. The two images are then combined into a single false-color image of 768 × 576 pixels and displayed at video frame rate. In fluorescence mode the image of endogenous fluorescence is normalized by the image of reflected red light to minimize the effects of varying tissue distance and viewing angle or shadowing. Due to intensity variations in fluorescence emitted by various bio-tissues, the normal tissue appears in shades of cyan, while abnormal tissue appears in shades of red color. The central 16 × 12 pixels are averaged over four frames and continuously displayed on the fluorescence image online screen as a numerical color value (NCV) (Fig. 2(B), in the centre). The higher the

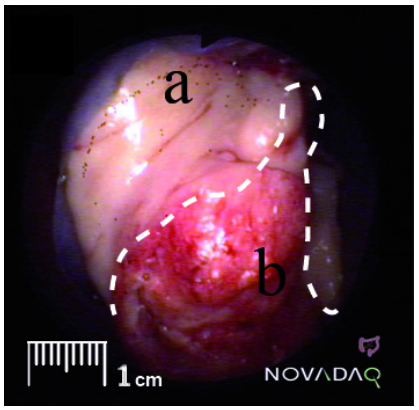

(A)

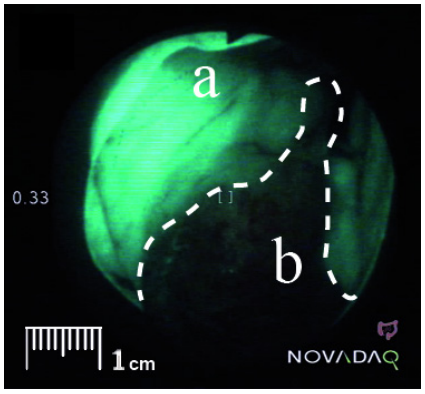

(B)

Fig. 2. White light (A) and autofluorescence (B) images of human jaw tissue under examination before laser ablation; a — Normal and b — Cancer. The white dashed line is a guidance provided by the surgeon as a boundary of the cancer lesion (Ab) matching the delineation provided by the autofluorescence image (Bb). The cancer diagnosis was confirmed by the pathologist. The ruler bar (1 cm) represents actual dimensions.

NCV, the lower the fluorescence intensity (associated with neoplasia): hence high NCVs help confirm the abnormality of lesions seen on the fluorescence image. Technical details regarding the device are described elsewhere.[18,19] A conventional fiber gastroscope (GIF-Q20, Olympus Corporation, Japan) was used for image collection. We used a color frame grabber (DT3120, Data Translation Inc., USA) that features an external trigger which is coupled with the PinPoint^{TM} camera controller via a foot-switch. Monitoring, triggering, and capturing of the video frames was controlled by our own scripts written in Matlab (R2007b, Mathworks Inc., USA). Images of 768 × 576 pixel resolution were obtained in tiff format. The color channels of the composite images (red, green, and blue) were filed separately for the conventional white light imaging mode (Fig. 2(A)) and for the fluorescence imaging mode (Fig. 2(B)). The full-color images of white light and fluorescence are 24-bit images each, with eight-bit information per channel (red, green, and blue). An additional image processing method was applied to observe the differential image $D = A(r) - B(g)$ between the red color channel of the white light image $A(r)$ and green channel of the fluorescence image $B(g)$. The D-image was linearly scaled such that its pixel values fit into the range 0–255, which is common for grayscale image formats. Then we coded the grayscale image of each green eight-bit channel, substituting the 256 levels of gray (0–255) using the RGB-rainbow lookup table (color bar on Fig. 4). An Er:YAG laser (2.94 μm, Glissando, WaveLight^{TM}, Germany) was used to cause laser ablation on both normal and cancer sites of the specimen. The pulse duration was 350 μs, power (per pulse) – 20 Watt, focus spot diameter — 0.377 mm. The autofluorescence was also collected in the red range (610–750 nm emission, 500–600 nm excitation) exploiting a fiberoptic spectrometer QE-6500^{TM} (Ocean Optics, USA), long pass interference filter from Thorlabs, 1.8 mm diameter bifurcated seven-fiber probe (MSL-RP6-1-200^{TM}; Medspeclab, Canada). The light from the endoscopic light source was used for the fluorescence excitation. Two specimens were taken from the lower jaw of the patients including soft and hard tissues under conditions of the ethical protocol approval for preliminary studies. The study was followed by histological examination by the pathologist to delineate the precise lesion boundary as it was visually estimated by the surgeon first.

3. Results

The primary results are shown in Figs. 2 and 3. White light and autofluorescence images of human jaw tissue before and after ablation are shown on Figs. 2(A), 2(B), 3(C), and 3(D) accordingly; a and b are the areas of normal and cancerous tissue and the small white and black circles added on the images indicate the actual ablation crater loci. In the white light image normal tissue areas retain their color during ablation while cancerous areas reduce their redness and tend to appear closer to the colors of normal tissue. These color changes of abnormal tissue translate to increases in intensity in the fluorescence image after ablation. These brighter areas extend beyond the actual sizes of the ablation craters which are indicated by the black

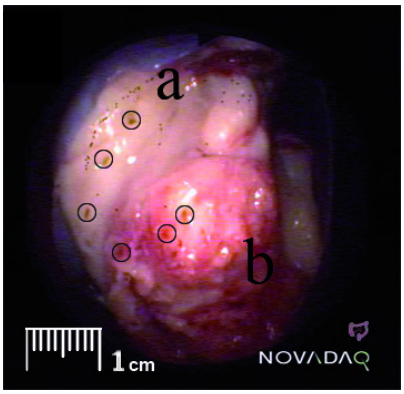

(C)

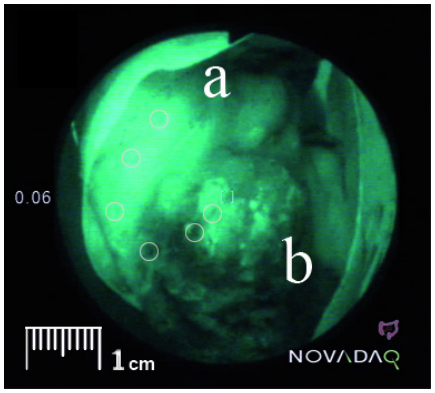

(D)

Fig. 3. White light (C) and autofluorescence (D) images of human jaw tissue after ablation are shown on C and D, a — Normal and b — Cancer. The ruler bar (1 cm) represents actual dimensions.

and white circles. A comparison between Figs. 2(B) and 3(D) shows that after the laser ablation the fluorescence image appears brighter or "healthier" not only within the normal tissue but also inside the cancer lesion sites. This observation is supported by the digital representation of NCV in the malignant area before ($NCV_{before} = 0.33$) and after ($NCV_{after} = 0.06$) the laser ablation. The histological examination has shown that this area is a cancer tissue. The existing technology implemented in PinPoint^{TM} for distinguishing between cancerous and normal tissue via green fluorescence emission, which is normalized by red reflectance, fails under conditions of high laser power effects on biological tissues. The differential images D before (A) and after (B) ablation are presented in Figs. 4(A) and 4(B). In these images cancerous tissue (bright, red) can still be distinguished from normal tissue (dull, green) on a large scale. However the boundary here between the normal and cancerous areas is distorted. The autofluorescence spectra acquired within the red part of the spectrum are depicted in Fig. 5. The contrast between normal and cancerous tissues is still present after the laser ablation, but it is reduced from 1:10 (A) to 1:2 (B). A similar analysis of the second sample confirmed the observations of the first specimen.

4. Discussion

The high power tissue processing alters the optical properties of the tissue, which is described in literature.[9,20] Our present model of these alterations is illustrated in Figs. 1(A) and 1(B). We expected the fluorescence of the tissue to recover within the ablation craters after the lesion removal. At malignancy, the thick mucosa and cancer angiogenesis lead to a high absorption of excitation light and re-absorption of the fluorescence emission, which

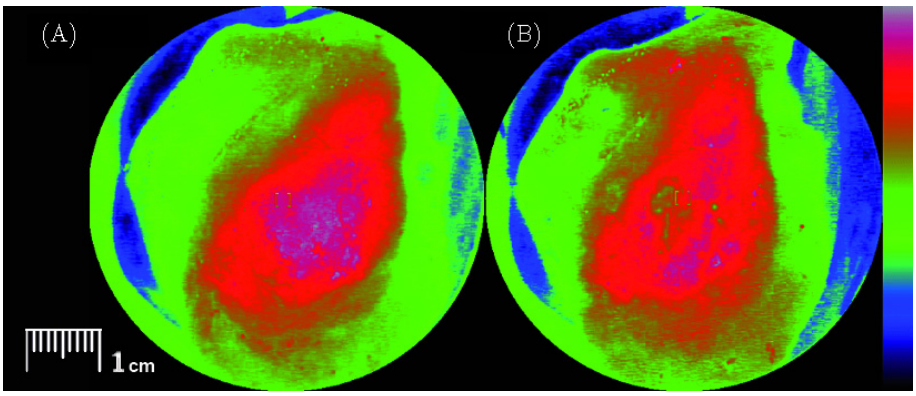

Fig. 4. False-color (RGB-rainbow lookup table, the color scale bar is presented on the right) differential D images before (a) and after (b) ablation. Here cancerous tissue (bright, red) can still be distinguished from normal tissue (dull, green) on a large scale. However the boundary between normal and abnormal areas remains altered. The ruler bar (1 cm) represents actual dimensions.

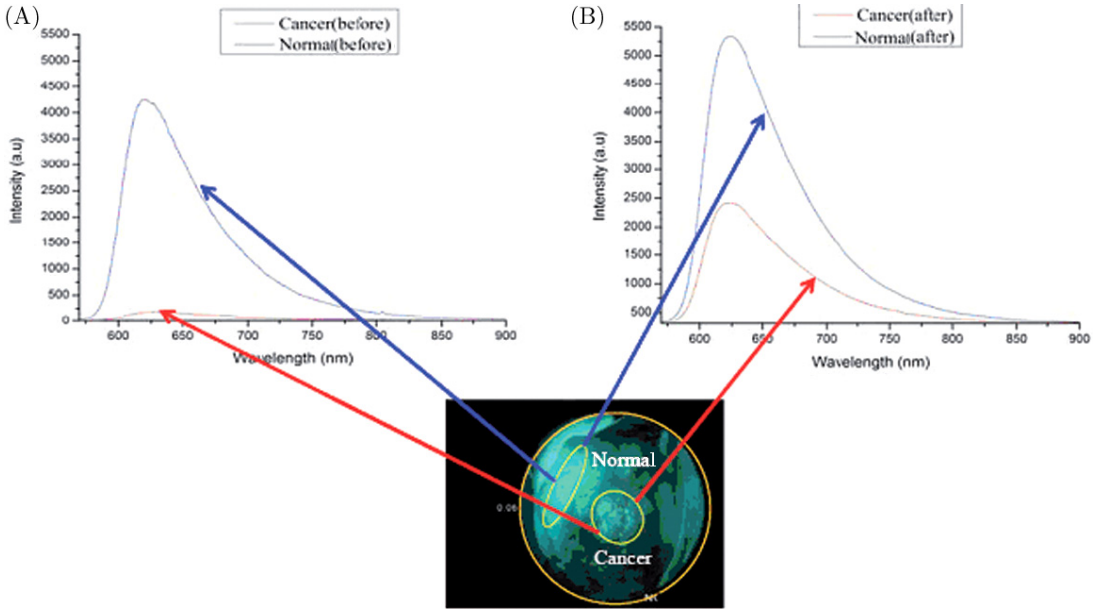

Fig. 5. Fiberoptic spectrometry of red autofluorescence. The red autofluorescence was measured by a fiberoptic spectrometer before (A) and after laser ablation (B). The fiber tip collected the spectra at the tissue spots indicated by the blue and red arrows in the fluorescence image. Cancer is represented by the red curve, while normal is the blue curve. The green fluorescence image is shown only for orientation. The contrast of cancerous vs normal tissue remains after the laser surgery, even though it is significantly reduced. The contrast reduced from 1:10 (A) to 1:2 (B).

is believed to be the cause of the contrast before ablation. According to the main hypothesis of the study, once such light shield is removed, the autofluorescence enhances and the contrast disappears or becomes reduced. In other words, the laser ablation "drills" the tissue down to the layers underneath the crater (usually the connective tissue), which are rich in fluorophores. The tissue autofluorescence increases and hence the contrast between normal and abnormal areas is reduced. Around the crater rim we expect formation of coagulation zones due to the tissue thermoconductivity. At coagulation the scattering increases and autofluorescence drops,[9–13] thus even improving the normal/abnormal contrast. However, we have found out that normal tissue areas retain their color during ablation while cancerous areas reduce their redness and tend to appear closer to the colors of normal tissue. As it is shown in Fig. 2(B) vs 3(D), the fluorescence growth beyond the crater rims takes place both in normal and cancerous tissues. Nevertheless in normal tissue such contribution is relatively minor due to the high initial level of the autofluorescence. We hypothesize that the main reason of this phenomenon is absorption and scattering changes of the epithelial tissue due to its heating outside the actual ablation crater. The epithelium is located above the fluorophor rich layers and may undergo a certain optical clearing due to the hyperthermia under conditions of pulse irradiation.[14–16] If the fluorophor such as collagen underwent coagulation then its fluorescence would drop down with increasing temperature,[17] however this effect has not been observed in our study. We have not performed direct measurements to monitor or assess tissue coagulation or denaturation in this preliminary study. It is planned in our future research.

The differential image between the red channel of the white light and green channel of the fluorescence image displayed restoration of the bulk normal/abnormal contrast but cannot provide fine margin delineation. From a system theoretic perspective image or matrix D essentially constitutes the negative biases of linear systems $B = B(A) = A - D$, which were excited by illumination A and responded with fluorescence B. These systems, which are locally distributed throughout the observed tissue surface, presumably change their biases according to the type of tissue beneath the surface. Another simple model of the relationship between A and B is $B = B(A) = Q \times A$, which essentially interprets the local tissue as an amplifier Q rather than a bias generator D. A much more sophisticated approach for such black box modeling of IO behavior, however, would be also to look at tissue dynamics of tissue responsiveness,

uncovering how excitation translates to fluorescence in terms of attenuation and phase over frequency. To identify model or system parameters then would require taking image sequences while exciting the tissue with variable illumination intensities. Such dynamic (instead of static) modeling of the relationship between A and B, which essentially yields a set of linear differential equations, might potentially reveal internal tissue dynamics and their change patterns due to laser processing. Such information might offer more abundant ways to safely classify the type of tissue than the current state of the art. Equipment which allows for the identification of such general models or relationships would then have to be able to shoot image sequences at higher frame rates than the used system can and would have to allow for changing illumination with each image frame taken. Such signal processing however is beyond the scope of this work. However, fast algorithms to identify the parameters of linear nth order models are readily available.[21]

The red fluorescence, usually associated with mitochondria or lysocomes,[22] was found significantly lower in cancer lesions. This contradicts the literature on red fluorescence level of cancer lesions in stomach and lungs *in vivo*,[23,24] and may be related to the surgery preparation in the mouth cavity as well as to the *ex vivo* conditions. The fluorescence spectra in Figs. 5(A) and 5(B) show that the normal/abnormal contrast in red fluorescence images remains after laser ablation and this may be an indication of a mechanism differing from that shown in Fig. 1. As such, it may potentially be optimized and used for surgical navigation due to the better stability of the normal/abnormal contrast after laser ablation.

5. Conclusions

The tumor tissue after the laser ablation increases in brightness when using the existing technology of distinguishing between cancerous and normal tissue. The current technology uses images of green fluorescence emissions which are normalized by reflected red light. It fails under conditions of high laser power effects on biological tissues. The study has shown a certain prospective image color channel manipulation to restore the normal/abnormal contrast after ablation. However, when the autofluorescence was collected in the red range (630–690 nm) then the abnormal/normal contrast did not decrease below levels that are usable for laser tissue processing. The present study highlights the importance of finding a proper technology for surgical navigation of cancer removal under conditions of high power effects in biological tissues. In future studies we are going to explore bio-tissue fluorescence in an attempt to identify models that relate photo-excitation with fluorescent emission and that allow for robust classification of tissues under laser treatment. Since simple models, such as the differential images, can well be identified with current technology, one focus will be to uncover the potential of such models. Another focus will be to capture optical tissue properties including absorption, scattering, and excitation–emission matrices (EEM) before and during the laser surgery within the visible range in order to find ways to improve concurrent technology for surgical navigation under high power effects.

Acknowledgments

The authors gratefully acknowledge funding of the Erlangen Graduate School in Advanced Optical Technologies (SAOT) by the German National Science Foundation (DFG) in the framework of the excellence initiative and Bavarian Laser Centre (BLZ) for support of this study.

References

1. E. Moriyama, A. Kim, A. Bogaards, L. Lilge, B. Wilson, "A ratiometric fluorescence imaging system for surgical guidance," *Adv. Opt. Technol. 2008*, Article ID 532368 (2008).
2. Y. Takeuchi, N. Uedo, R. Ishihara, H. Iishi, "Is narrow band imaging with magnifying endoscopy useful for the estimate of tumor lateral extent before endoscopic submucosal dissection for early gastric cancer? — A retrospective analysis compared with chromoendoscopy," *Gastrointest. Endosc.* **67**(5), AB277–AB278 (2008).
3. J. Schipper, A. Berlis, T. Klenzner, A. Schramm, N. Gellrich, S. Rosahl, W. Maier, "Navigationsunterstützte tumorfokussierte Chirurgie bei Schädelbasismalignomen — Zusätzlicher chirurgischer Manipulationsraum durch neoadjuvante Tumorverkleinerung (Navigated "targeted surgery" for skull base öpmalignomas — Aditional space for surgical manipulation by neoadjuvant tumor downsizing)," *HNO* **55**(6), 465–471 (2007).
4. T. Itoi, S. Tsuji, A. Sofuni, F. Itokawa, T. Kurihara, T. Tsuchiya, K. Ishii, N. Ikeuchi, M. Igarashi, T. Gotoda, "A novel approach emphasizing preoperative margin enhancement of tumor of the

major duodenal papilla with narrow-band imaging in comparison to indigo carmine chromoendoscopy (with videos)," *Gastrointest. Endosc.* **69**(1), 136–141 (2009).

5. R. Kiesslich, M. Neurath, "Endoscopic detection of early lower gastrointestinal cancer," *Best Pract. Res. Clin. Gastroenterol.* **19**(6), 941–961 (2005).
6. N. Fujioka, Y. Morimoto, T. Arai, M. Kikuchi, "Discrimination between normal and malignant human gastric tissues by Fourier transform infrared spectroscopy," *Canc. Detect. Prev.* **28**(1), 32 (2004).
7. G. Wagnieres, W. Star, B. Wilson, "In vivo fluorescence spectroscopy and imaging for oncological applications," *Photochem. Photobiol.* **68**(5), 603–632 (1998).
8. R. Dacosta, B. Wilson, N. Marcon, "New optical technologies for earlier endoscopic diagnosis of premalignant gastrointestinal lesions," *J. Gastroenterol. Hepatol.* **17**(Suppl), S85–S104 (2002).
9. J. Ritz, A. Roggan, C. Germer, C. Isbert, G. Muller, H. Buhr, "Continuous changes in the optical properties of liver tissue during laser-induced interstitial thermotherapy," *Lasers Surg. Med.* **28**(4), 307–312 (2001).
10. K. Mahlstedt, U. Netz, D. Schädel, H. Eberle, M. Gross, "An initial assessment of the optical properties of human laryngeal tissue," *ORL* **63**(6), 372–378 (2000).
11. M. Ith, M. Frenz, H. Weber, "Scattering and thermal lensing of 2.12-m laser radiation in biological tissue," *Appl. Opt.* **40**, 2216–2223 (2001).
12. A. Croce, S. Fiorani, D. Locatelli, R. Nano, M. Ceroni, F. Tancioni, E. Giombelli, E. Benericetti, G. Bottiroli, "Diagnostic potential of autofluorescence for an assisted intraoperative delineation of glioblastoma resection margins," *Photochem. Photobiol.* **77**(3), 309–318 (2003).
13. L. I. Deckelbaum, M. L. Stetz, K. M. O'Brien, F. W. Cutruzzola, A. F. Gmitro, L. I. Laifer, G. R. Gindi, "Fluorescence spectroscopy guidance of laser ablation of atherosclerotic plague," *Lasers Surg. Med.* **9**(3), 205–214 (1989).
14. C. T. Piazza, "Method and device for treating tissue using a coagulated beam path," US Patent Application 20080255639 from 10-16-2008.
15. P. O. Rol, "Optics for transscleral laser applications: Dissertation No. 9655 for Doctor of Natural Sciences," Swiss Federal Institute of Technology, Zurich, Switzerland (1992).
16. V. V. Tuchin, *Optical Clearing of Tissues and Blood*, PM 154, SPIE Press, Bellingham, WA (2006).
17. J. M. Menter, "Temperature dependence of collagen fluorescence," *Photochem. Photobiol. Sci.* **5**, 403–410 (2006).
18. A. Douplik, S. Zanati, N. Marcon, M. Cirocco, B. Wilson, J. Boehm, S. Rychel, J. Fengler, "Combined autofluorescence and white-light endoscopy for improved detection of dysplastic colonic lesions," in *Biomedical Optics, Technical Digest (CD), Optical Society of America*, paper ME63 (2006).
19. A. Douplik, W. Leong, A. Easson, S. Done, G. Netchev, B. Wilson, "Feasibility study of autofluorescence mammary ductoscopy," *J. Biomed. Opt.* **14**(4), 044036 (2009).
20. H. Ao, D. Xing, H. Wei, H. Gu, G. Wu, J. Lu, "Thermal coagulation-induced changes of the optical properties of normal and adenomatous human colon tissues in vitro in the spectral range 4001100 nm," *Phys. Med. Biol.* **53**(8), 2197–2206 (2008).
21. R. Hohenstein, "Entwurf hochdynamischer Sensor- und Regelsysteme für die adaptive Laserbearbeitung," *Reihe Fertigungstechnik* **151** (2004).
22. H. Stepp, R. Sroka, R. Baumgartner, "Fluorescence endoscopy of gastrointestinal diseases: Basic principles, techniques, and clinical experience," *Endoscopy* **30**(4), 379–386 (1998).
23. V. Loschenov, M. Baryshev, M. Kuzin, V. Zavodnov, L. Uspensky, U. Ablitsov, L. Loginov, V. Rybin, "Spectral-autofluorescent diagnostics of stomach and lung cancer," *Proc. SPIE* **1641**, 177 (1992).
24. S. Lam, C. MacAulay, B. Palcic, "Detection and localization of early lung cancer by imaging techniques," *Chest* **103**, 12–14 (1993).